Electronic Properties of Light- and Elevated Temperature-Induced Degradation in Float-Zone Silicon

Zhuangyi Zhou, Mattias Klaus Juhl, Michelle Vaqueiro-Contreras, Fiacre Rougieux, and Gianluca Coletti

Abstract—Light- and elevated temperature-induced degradation (LeTID) causes long-term instabilities, especially in passivated emitter and rear cells, leading to severe performance loss of commercial modules. Despite the hundreds of LeTID reports available in the literature, there is little consensus regarding the underlying defects and defect formation mechanism responsible for this degradation and its exact electronic properties. Recently, it has been shown that a form of carrier-induced degradation similar to that of LeTID is also observed in some high-purity silicon crystals grown by the float-zone method. In this work, using deep level transient spectroscopy and lifetime spectroscopy, we study the role of nitrogen on the degradation. Intentional contaminated samples with different and known level of nitrogen have been specially grown and characterized for this study. We detect the appearance of a set of majority carrier traps in the degraded state of the samples with activation energies 0.1 (H85), 0.43 (H270A), 0.39 (H270B), and 0.46 eV (H200) with respect to the valence band, from which H270A appears to correlate with the degradation. The results show that the extent of degradation in the nitrogen-rich samples is at least double that of the nitrogen-lean samples.

Index Terms—Deep level transient spectroscopy (DLTS), defects, degradation, float-zone (FZ), light- and elevated temperature-induced degradation (LeTID), nitrogen, quasi-steady-state photoconductance (QSSPC), silicon.

I. INTRODUCTION

LIGHT- and elevated temperature-induced degradation (LeTID) is one of the most severe degradation mechanism in passivated emitter and rear cells. LeTID was first observed in multicrystalline silicon (mc-Si) by Ramspeck et al. [1]. Later, Fertig et al. [2] and Chen et al. [3] showed that the same degradation mechanism affects not only mc-Si but also monocrystalline
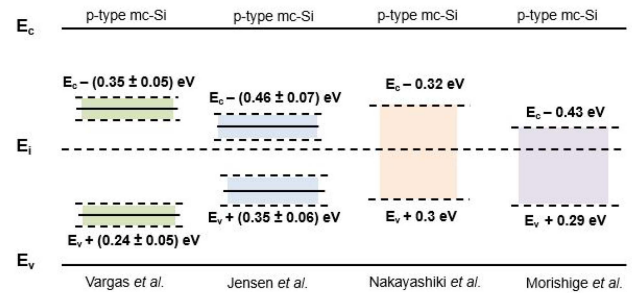
Fig. 1. Previously reported LeTID-related defect energy levels using lifetime spectroscopy [8], [11]–[13].

silicon (mono-Si). Chen et al. [3] showed evidence of a defect in p-type Czochralski silicon (Cz-Si) behaved similarly, and more recently in n-type Cz-Si that underwent boron diffusion [4]. Niewelt et al. [5] and Sio et al. [6] also observed a similar degradation phenomenon in p-type float-zone (FZ) silicon and cast mono-Si, respectively. Therefore, LeTID appears to be fundamentally present or introduced in all silicon materials [7]. Moreover, several studies [5], [7]–[10] suggest that hydrogen is involved in LeTID-related defect formation.

Several publications examined the electronic properties of the defect(s) responsible for LeTID using lifetime spectroscopy [8], [11]–[13]. Some of the energy levels reported in the literature are shown in Fig. 1. The reported results using lifetime spectroscopy are scattered over a relatively wide range, with some studies suggesting the existence of a single midgap level [12], [13], whereas other studies suggest the presence of two levels [8], [11]. Moreover, the absolute values of the capture cross sections remain unknown as lifetime spectroscopy can only measure capture cross section ratios. Nevertheless, to predict the impact of LeTID in actual solar cell devices, understanding the electronic structure of LeTID-related defect(s) is critical. Until recently, only three studies have investigated the electronic properties of LeTID-related defect(s) using deep level transient spectroscopy (DLTS). Two minority carrier traps at E_c-0.19 eV and E_c-0.34 eV were detected in degraded mc-Si solar cells and ascribed to LeTID-related defects [14]. A majority carrier trap at E_v+0.42 eV was also found in mono-Si solar cells subjected to outdoor LeTID conditions [15]. In addition, an electron emission signal with activation energy of approximately 0.175 eV was detected by DLTS, and it was suspected to be linked to LeTID [16].

TABLE I
P-DOPED AND B-DOPED N-RICH AND N-LEAN FZ SAMPLE INFORMATION

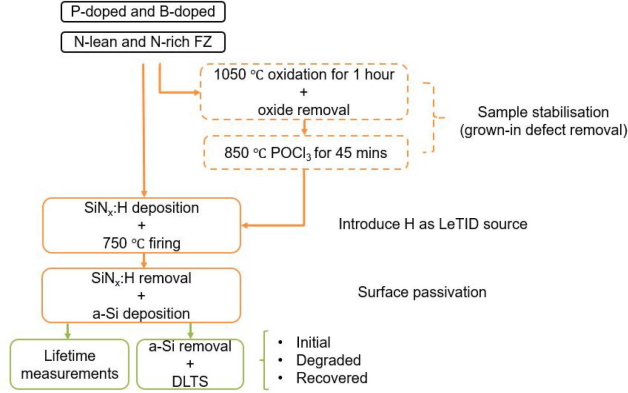| Sample label	Thickness (μm)	Resistivity (Ω·cm)	[O] (cm^{-3})	[N] (cm^{-3})
N-rich	290±10	3-5	$< 2 \times 10^{16}$	$\sim 6 \times 10^{14}$
N-lean	290±10	3-5	$< 2 \times 10^{16}$	$\sim 2 \times 10^{14}$

Fig. 2.   Experiment processes and the corresponding purposes.

However, these results were measured in relatively defect-rich materials (mc- and Cz-Si), which can point to other defects besides LeTID defects, and the analysis of the capture cross sections was performed using Arrhenius plots rather than from direct capture measurements using reverse bias filling pulses that provides the actual capture cross section. In this work, the capture cross sections and activation energy levels of LeTID-related defects are measured in, otherwise, defect-lean FZ silicon. In particular, the role of nitrogen is studied in samples intentionally grown with two different nitrogen contents. Nitrogen enables high-quality FZ silicon growth but can also lead to the formation of electrically active deep level defects in certain conditions [17]–[19]. In this study, we investigate the relationship between LeTID and nitrogen and the electronic properties of LeTID via DLTS. The capture cross sections are measured via variable reverse bias pulse fillings instead of Arrhenius measurements.

II. EXPERIMENTAL DETAILS

The sample details are tabulated in Table I, and the design of the experiment is shown in Fig. 2. In this work, 3–5 Ω·cm N-rich and N-lean, P-doped (n-type), and B-doped (p-type) FZ silicon wafers from Topsil were used. Nitrogen was introduced during the silicon ingot growth process. The nitrogen content is usually above 1×10^{14} cm^{-3} in FZ silicon and up to the solubility of around 4.5×10^{15} cm^{-3} [20]. Previous studies show that nitrogen can prevent the formation of extended defects [17]–[19], for instance nitrogen suppresses the formation of vacancy and interstitial aggregates in FZ silicon [17], [18]. In addition, nitrogen also pins dislocation, thus increasing the mechanical strength of silicon wafers [21]. Despite the advantages of nitrogen, it can also form electrically active deep level defects upon annealing [22]–[25]. Thus, a stabilization process known to remove grown-in defects in FZ silicon was used on half of

the samples (dashed boxes shown in Fig. 2). The stabilization process consisted of a 1 h oxidation step at $\sim 1050°$C followed by a 45 min gettering (after oxide removal) at $\sim 850°$C with POCl$_3$ [26].

Half of the stabilized 100 mm diameter FZ wafers were then processed as follows: after the silicate glass and the diffusion layer removal, a 75 nm thick SiN$_x$:H layer with a reflective index of 2.08 at 633 nm [27] was deposited on both sides using a Meyer Burger MAiA remote-PECVD tool, followed by a fast-firing step at a measured peak temperature of $\sim 750°$ C using an in-line Schmid metallization belt furnace with a set conveyor speed of 4.5 m/min. Next, SiN$_x$:H layers were removed with HF due to nonideal passivation and then a 20 nm Amorphous silicon (a-Si) layer was deposited on both sides of the wafers using an Oxford Instruments plasmalab 100 PECVD system at 300° C for 30 s for surface passivation.

After the abovementioned steps, the wafers were cut into small samples from each group for DLTS measurements and the remaining samples were used for in-situ minority carrier lifetime measurements during LeTID treatment. Lifetime measurements were performed using quasi-steady-state photoconductance measurements with a photoconductance tool (Sinton Instruments, WCT-120TS [28]) at a temperature of $\sim 75°$C, via an additional LED with absorbed photon flux of 1.78×10^{17} cm^{-2}s^{-1} leading to a steady-state illumination corresponding to about 1 kW/m^2 in between lifetime measurements. Three samples from each group were cleaved for DLTS measurements, including one as manufactured sample in the initial state; the remaining samples were processed alongside the lifetime monitoring sample with the a-Si passivation layers still on, with one sample being removed from the LeTID process when the maximum lifetime degradation was observed for DLTS measurement. Next, the last passivated sample was subjected to a further ~ 75 h after maximum degradation under the same LeTID treatment until the recovered state was reached and measured with DLTS. In preparation for DLTS measurements, the samples were dipped in HNO$_3$ (70%): HF (49%): H$_2$ O = 25: 1: 25 solution for 1 min in order to remove the a-Si layer, followed by ultrasonic cleaning in Acetone and then IPA for 5 min, respectively. The samples were HF dipped prior to metal evaporation for oxide removal. Finally, aluminum was thermally evaporated with a 1-mm diameter circle shadow mask to form Schottky contacts on the front, and Gold on the back for Ohmic contacts for p-type FZ samples, and vice versa for n-type.

III. EXPERIMENTAL RESULTS

A. Analysis of Lifetime Measurements

We have performed lifetime measurements to investigate the impact of nitrogen on the formation kinetics and maximum extent of LeTID in our samples. The samples were degraded under a light intensity of around 1 kW/m^2 and a temperature of 75°C, analogous to previous LeTID treatments on p-type FZ silicon wafers [5], which we henceforth will refer to as the LeTID formation process. Using such a condition, we observed a significant lifetime degradation on our p-type samples but no lifetime degradation on the n-type material, which is in
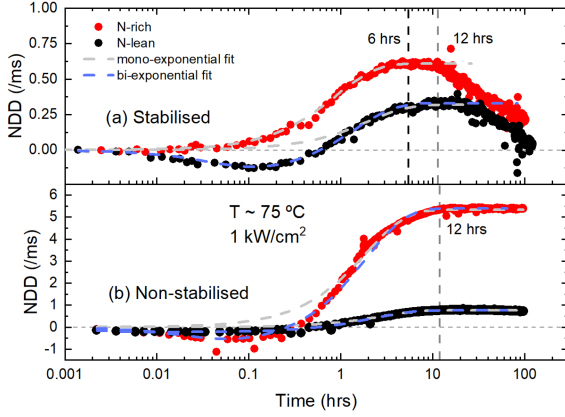
Fig. 3. Normalized defect density as a function of light soaking time on (a) stabilized and (b) nonstabilized p-type FZ silicon at an injection level of about $\Delta n = 5 \times 10^{14}$ cm^{-3} (~10% doping).
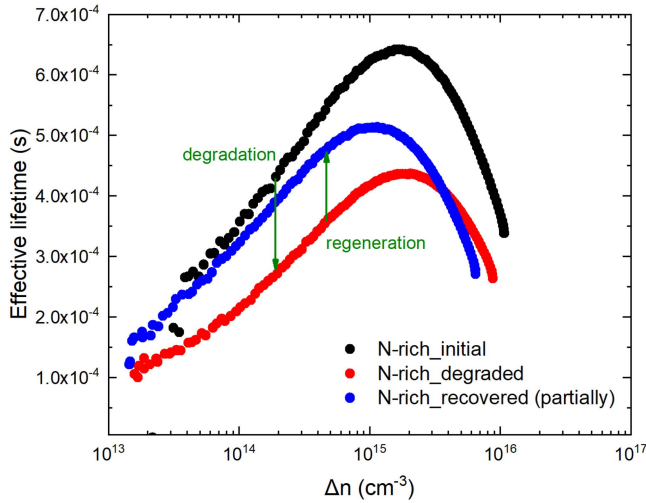

Fig. 4. Effective lifetime as a function of excess carrier density of the stabilized N-rich samples in its initial, degraded and partially recovered (~60 h during the LeTID formation process) states.

agreement with previous reports [5]. Therefore, we focus on the B-doped FZ samples in this article.

To evaluate the impact of LeTID, we used the apparent normalized defect density (NDD) metric, defined as [29]

$$N_{NDD}(\Delta n) = \frac{1}{\tau_{eff}(\Delta n)} - \frac{1}{\tau_{initial}(\Delta n)} \tag{1}$$

where $\tau_{eff}(\Delta n)$ is the lifetime measured during the LeTID formation process at an injection level Δn, and $\tau_{initial}(\Delta n)$ is the lifetime extracted in the beginning of the LeTID formation process at the same injection level Δn. NDD is evaluated at an injection of 5×10^{14} cm^{-3} (~10% doping).

The resultant NDD values as a function of light soaking time for the p-type FZ silicon samples are shown in Fig. 3. As shown in Fig. 3(a), the maximum NDD for the stabilized N-rich FZ sample is approximately twice that of the stabilized N-lean FZ sample. Fig. 4 shows the effective lifetime of the N-rich sample in its initial, degraded, and partially recovered states (~60 h under LeTID formation process). Note that the

TABLE II
NORMALIZED DEFECT DENSITY AND DEGRADATION RATES OF N-RICH AND N-LEAN SAMPLES THAT UNDERWENT A STABILIZATION PROCESS

Monoexponential fit	N-rich	N-lean	Ratios (rich/lean)
Max NDD (1/ms)	0.6	0.3	2.0
Degradation rate (1/h)	1.1	0.5	2.2
Bi-exponential fit	N-rich	N-lean	Ratios (rich/lean)
Level 1 max NDD (1/ms)	0.6	0.5	1.2
Level 1 degradation rate (1/h)	1.1	0.7	1.6
Level 2 max NDD (1/ms)	-	0.2	-
Level 2 improvement rate (1/h)	-	22.0	-

difference in NDD is not affected by the surface recombination as no significant difference in the dark saturation current ($J0$) at an injection level of 1×10^{16} cm^{-3} is observed during the LeTID formation process. From Fig. 3(a), the negative NDD in the beginning is due to an initial lifetime increase in the N-lean sample, analogous to that measured by Sperber et al. [30].

It is likely that another defect level [Level 2 as indicated in the following in the biexponential fit with (3)] is deactivated and resulting in the lifetime increase. Fe (as measured using a flash and lifetime measurements) is not detected in our samples [31]. The nature of the deactivated defect remains unknown and may be related to that observed by Chan et al. [32], whereas short dark annealing applied prior to the LeTID formation process results in the changes of the degradation kinetics. Note that only the N-lean stabilized sample shows an initial decrease in NDD. One possible explanation is that the N-lean stabilized sample contains more intrinsic defect to be passivated. Nitrogen is known to bind to intrinsic defects and reduce extended defects [17]–[19]. The pool of defects that are able to be passivated in the initial stage of the process is, thus, greater in the N-lean samples [33].

We fitted the defect formation kinetics with a single exponential equation for the stabilized N-rich sample, and both, single and biexponential equations, for the stabilized N-lean sample as the biexponential equation for N-lean sample provides better quality fitting. The fitted parameters are tabulated in Table II. The formula used for single exponential fit is

$$N_{NDD} = N_{NDD(max)} \times [1 - \exp(-r_{deg} \times t)] \tag{2}$$

where $N_{NDD(max)}$ is the maximum NDD value, r_{deg} is the degradation rate, and t is the time in hours during the LeTID formation process.

The equation used for biexponential equation fit is

$$N_{NDD} = N_{NDD(max1)} \times [1 - \exp(-r_{deg} \times t)] \\ + N_{NDD(max2)} \times [\exp(-r_{imp} \times t) - 1] \tag{3}$$

where $N_{NDD(max1)}$ and $N_{NDD(max2)}$ are the maximum NDD values of the degradation and improvement, respectively, r_{deg} and r_{imp} are the degradation rate and the improvement rate, respectively, and t is the time in hours during the LeTID formation process.

The formation of LeTID defect is 1.6–2.2 times faster in the N-rich samples than in the N-lean samples (using single or biexponential fits) with larger maximum degradation extent as shown in Fig. 3(a), and tabulated in Table II. Note that the initial lifetime of the stabilized N-rich samples is about 1.4 times higher

TABLE III
NORMALIZED DEFECT DENSITY AND DEGRADATION RATES OF N-RICH AND
N-LEAN SAMPLES WITHOUT A STABILIZATION PROCESS

Monoexponential fit	N-rich	N-lean	Ratios (rich/lean)
Max NDD (1/ms)	5.3	0.8	6.6
Degradation rate (1/h)	0.5	2.8	0.7
Bi-exponential fit	N-rich	N-lean	Ratios (rich/lean)
Level 1 max NDD (1/ms)	6.2	1.0	6.2
Level 1 degradation rate (1/h)	0.5	0.5	1.0
Level 2 max NDD (1/ms)	0.8	0.2	4.0
Level 2 improvement rate (1/h)	40.0	500.0	0.1

than that of N-lean samples at an injection level of 5×10^{14} cm⁻³. This is a likely explanation for the difference in the degradation rate.

In the case of the nonstabilized samples [shown in Fig. 3(b)], the initial lifetime of nonstabilized N-rich sample is about 6.8 times higher than the lifetime of nonstabilized N-lean samples. The degradation rate and the extent of LeTID is about 6–7 times larger in N-rich than in N-lean samples. Given the impact of injection on lifetime changes, the degradation rate of LeTID in the nonstabilized group is minor. However, the degradation extent is more pronounced in the nonstabilized group than in the stabilized group. Lifetime regeneration was not observed in the nonstabilized N-rich sample and ∼11% recovery of lifetime from the maximum NDD state was found in the nonstabilized N-lean samples within the time scale (100 h) in this experiment. Similarly, both mono- and biexponential fits for NDD in the nonstabilized group are shown in Fig. 3(b) and the parameters are tabulated in Table III. Note that the rate of LeTID formation depends linearly on the carrier density [34]. However, here the different injection levels between N-rich and N-lean cannot explain the saturation of the effective density at different values. The maximum NDD in N-rich samples is higher than in N-lean samples in the nonstabilized group. In addition, by comparing Tables II and III, the nonstabilized sample group shows a larger NDD, being one magnitude larger for the N-rich samples and 2–3 times more than the N-lean samples. This suggests the stabilization process suppresses LeTID defect formation.

B. Electronic Properties of the LeTID-Related Defect

The initial, degraded, and recovered states were measured with DLTS from 30 K to 300 K for stabilized samples. The degraded states for the N-rich and N-lean groups used for the DLTS measurements were taken after ∼6 and ∼12 h, respectively, based on the time they took to reach maximum degradation in Fig. 3(a). The DLTS spectra for the N-rich and N-lean samples are shown in Fig. 5. Two peaks were detected in the N-rich degraded samples with maximum at ∼85 and ∼270 K [labeled H85 and H270 in Fig. 5(a)]. The N-lean degraded samples showed a broader peak at ∼65 K (composed of two peaks at 50 and 85 K, respectively) in the DLTS spectra [shown in Fig. 5(b)]. At the end of the experiment, we placed the diodes from degraded samples under the same LeTID treatment for another ∼75 h and obtained the same results as for the recovered diodes shown. Fig. 5(b) shows that only the H50 trap remains after LeTID recovery. The activation energy of H50 is extracted
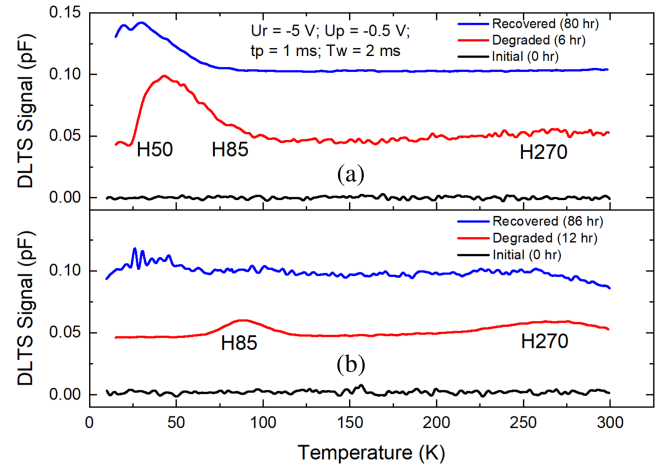

Fig. 5. DLTS results of stabilized (a) N-rich and (b) N-lean FZ silicon before degradation (initial), at maximum degradation (degraded), and after recovery (recovered). Measurement parameters [reverse bias voltage (UR), filling pulse voltage (UP), filling pulse lengths (TP), and period width (TW)] are listed in the graph. The spectra are shifted on the vertical axis for clarity.
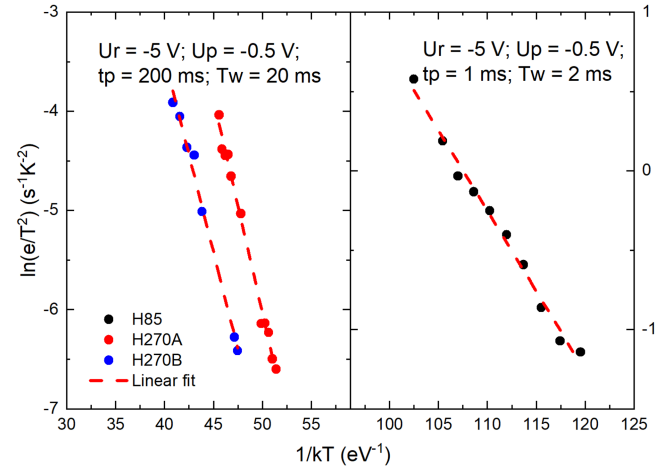

Fig. 6. Arrhenius plot of T^2-corrected emission rates of H85, H270A, and H270B. The red dashed lines are linear fits of the transient measurements.

from the Arrhenius plot as $E_t + E_\infty = 0.05$ eV. Since H50 is not observed in N-rich degraded samples, it is less likely to be related to the recombination active LeTID defect. Possible cause is that H50 could be related to vacancy or Si interstitial defects as N effectively suppresses the formation of vacancy and interstitial aggregates in silicon via $N_2 + V \rightleftharpoons N_2 V$ and $N_2 V + I \rightleftharpoons N_2$ [35].

The H85 and H270 traps were measured and analyzed in detail. Fig. 6 shows the temperature dependency of the emission rate for the H85 trap in the degraded N-rich sample. The rate of thermal emission of carriers from a trap at a certain temperature is defined as [36]

$$e_n = \sigma_n \upsilon_n N_c \cdot \exp\left(\frac{E_d}{kT}\right) \qquad (4)$$

where e_n is the thermal emission rate, υ_n is the thermal velocity of the majority carrier, N_c is the effective density of states of the conduction band, E_d is the apparent energy level for the
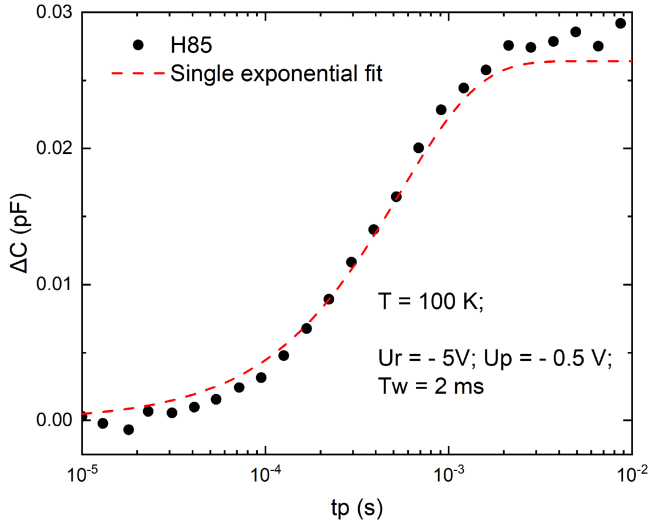
Fig. 7. Hole capture process of H85 at 100 K. The dashed line is a single exponential fit of the measured capacitance changes.

Fig. 8. Hole capture processes of the two traps under H270 at 240.5 K. Measurement parameters are included in the graph.

defect, k is the Boltzmann constant, and T is the temperature. Therefore, from the measured emission rates of the traps at their corresponding temperature ranges, their activation energies and apparent capture cross sections can be extracted from the slopes and the intercepts of the linear fits in the Arrhenius plot.

Under the assumption that the filling pulse (TP) is sufficiently long to fill the traps, the defect density extracted from the transients and CV results is calculated as [37]

$$\frac{\Delta C}{C_0} = \frac{N_t}{2N_d} \qquad (5)$$

where ΔC is the DLTS signal, C_0 is the initial capacitance without bias applied, N_t is the defect concentration, and N_d is the background dopant density.

The transient capacitance as a function of filling pulse duration in the degraded N-rich sample is shown in Fig. 7. For H85, we calculate an activation energy of 0.1 eV and an apparent capture cross section of 7.85×10^{-19} cm^2 based on the Arrhenius plot. Variable pulse filling measurements indicate an actual hole capture cross section of $\sim 2.83 \times 10^{-20}$ cm^2 for the H85 trap at 100 K. The defect concentration of H85 in the degraded state of the N-lean sample is 3.49×10^{13} cm^{-3}.

Using Laplace DLTS [38], peak H270 can be resolved into two separate traps. We extract the electronic properties of these two levels (H270A and H270B) from the Arrhenius plot, as shown in Fig. 6. The activation energy of trap H270A is 0.43 eV and its apparent capture cross section is 4.25×10^{-17} cm^2. The activation energy of trap H270B is 0.39 eV and its apparent capture cross section is 2.11×10^{-18} cm^2. The average defect densities of H270A and H270B are 9.55×10^{12} cm^{-3} and 1.07×10^{13} cm^{-3}, respectively. Note that for our system, the energy resolution is within the range of ± 10 meV, and the defect density sensitivity for these samples is approximately 4.0×10^{11} cm^{-3}.

The hole capture kinetics for H270A and H270B is shown in Fig. 8. The capture process of H270 at 240.5 K shows a biexponential nature. The filling rates are determined by fitting with two independent exponential equations shown in black and
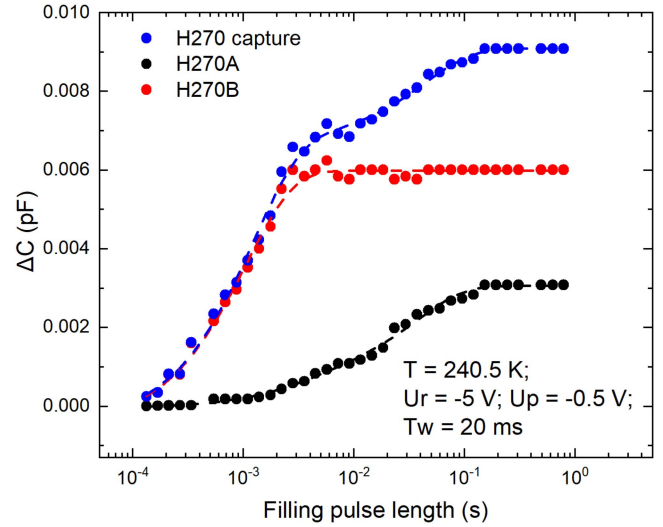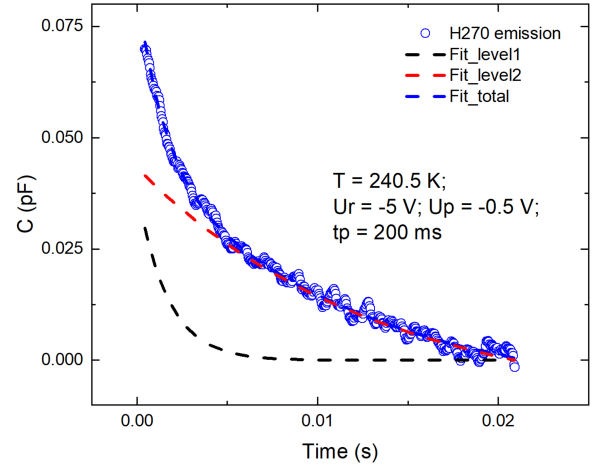

Fig. 9. Hole emission process of the two traps under H270 at 240.5 K. Measurement parameters are listed in the graph.

red dashed lines. The hole emission kinetics for H270 is shown in Fig. 9. The black and red dashed lines are the single exponential fits of the hole capture and emission processes of H270A and H270B, respectively, and the blue dashed lines is the sum of two single exponential fits. Again, the hole emission also shows the presence of two levels (using a filling pulse of 200 ms).

Analysis of the shape of the capture and emission capacitance data shows that the hole capture and emission of H270A and H270B are separated monoexponential processes, indicating that they are independent (not two levels of a multivalent trap). This is because the filling or emptying of one level does not depend on the occupation of the other level.

The electrical parameters and average defect concentration of H85, H270A, and H270B in the degraded B-doped FZ samples are tabulated in Table IV. The apparent capture cross section is extracted based on the slope of the corresponding hole emission in the Arrhenius plot, whereas the actual capture cross sections are calculated based on the measured capture rates.

TABLE IV
DEFECT PARAMETERS OF TRAPS IN THE DEGRADED B-DOPED FZ SAMPLE WITH STABILIZATION

Traps	H85	H270A	H270B
Activation Energy (eV)	0.10	0.43	0.39
Apparent capture cross section (cm^2)	7.85×10^{-19}	4.25×10^{-17}	2.11×10^{-18}
Filling pulse fitted capture cross section (cm^2)	2.83×10^{-20}	2.3×10^{-22}	1.96×10^{-22}
N-rich defect concentration (cm^{-3})	3.49×10^{13}	9.55×10^{12}	1.07×10^{13}
N-lean defect concentration (cm^{-3})	4.19×10^{13}	4.92×10^{12}	4.31×10^{12}
Defect concentration ratios (rich/lean)	0.83	1.94	2.48
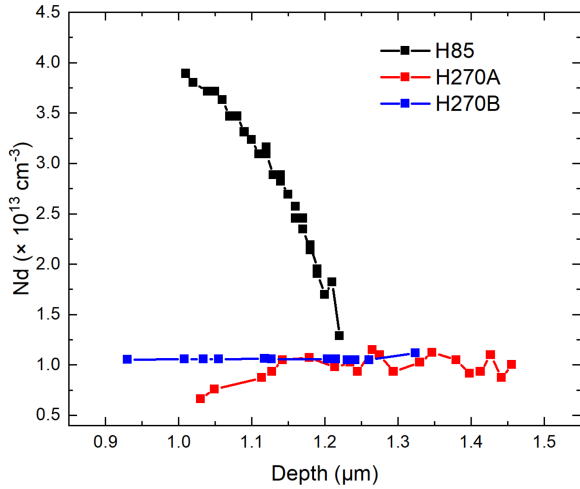
Fig. 10.　Depth profile of H85, H270A, and H270B in the stabilized N-rich sample.

Fig. 11.　Defect concentration of H85 in the stabilized N-rich sample measured continuously from low T to high T and then reversed.

The depth profile of all three traps detected by DLTS and the variation of H85 defect density (60–90 K) is shown in Fig. 10. All the defect concentrations in Fig. 10 are extracted from CV measurements with long filling pulse times (TP = 2 ms for H85 and TP = 200 ms for H270). The concentration of trap H270A and H270B does not vary with depth, as shown in Fig. 10, indicating they are likely to be bulk defects. On the other hand, H85 is more concentrated at the surface and may be a result of surface contamination. Another possibility may be that this trap is related to LeTID defects observed in previous studies via thickness-dependent lifetime measurements [10]. Since DLTS detects electrical active defects, H85 may be a gettered defect inline with the recombination inactive LeTID defect precursor (a metal–hydrogen complex) proposed by Schmidt et al. [10], which dissociates under illumination at elevated temperatures to form the recombination active LeTID complex. Further work is required to ascertain which of these two scenarios is more likely.

The defect density shown in Fig. 11 is extracted from CV measurements and the transient amplitude changes, depending on whether the measurement temperature is ramped up or down. This suggests that H85 is a metastable defect.

IV. DISCUSSION

In this section, we discuss the role of nitrogen introduced during silicon ingot growth on the formation of LeTID. We also investigate the electronic properties of LeTID-related defects.

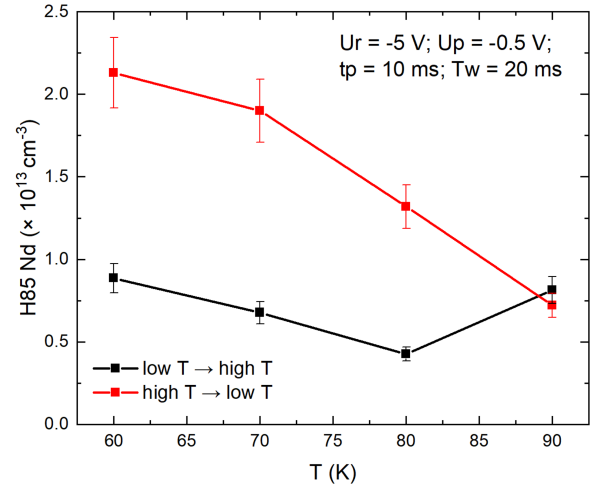From lifetime spectroscopy we observe that the N-rich samples display more severe bulk degradation than the N-lean samples during the LeTID formation process. The lifetime evolution in the nonstabilized N-rich sample is similar to LeTID but a decrease in NDD was not observed in the first 100 h, and only a ~11% reduction in NDD was observed in the nonstabilized N-lean sample within the first 100 h [see Fig. 3(b)]. Assuming the degradation and regeneration happen simultaneously during the LeTID formation process (e.g., [30]), the timescale to observe recovery in the lifetime changes could take up to months if the samples are not stabilized. The results in Fig. 3(b) show that LeTID regeneration is faster in the stabilized group. As the lifetime of our samples is lower than the other studies (e.g., [30]), the kinetics is correspondingly slower. This may explain why small lifetime recovery is only observed in the N-lean nonstabilized samples.

The stabilization process possibly contributes to effusion of nitrogen from the samples as demonstrated by Hiller et al.[39]. Assuming a diffusion coefficient of N-N pairs $D_p = 2.7 \times 10^3 \cdot \exp(-2.8 \, \text{eV}/kT) \, \text{cm}^2\text{s}^{-1}$ [40], all the nitrogen contained within the samples is likely to be effused as a result of the oxidation step (during the stabilization treatment). Nitrogen is known to interact with intrinsic defects, such as interstitials and vacancies [41]. The large difference in the maximum NDD between N-rich and N-lean samples in the nonstabilized group (factor of 6–7) suggests that nitrogen plays a role, directly or indirectly, in the samples' lifetime degradation. After stabilization, this ratio strongly decreases, with the degradation in the N-lean sample being much smaller in the nonstabilized case. The small difference (factor of 2) between N-rich and N-lean stabilized

TABLE V
TRAPS IN BOTH DEGRADED N-RICH AND N-LEAN SAMPLES WITHOUT STABILIZATION

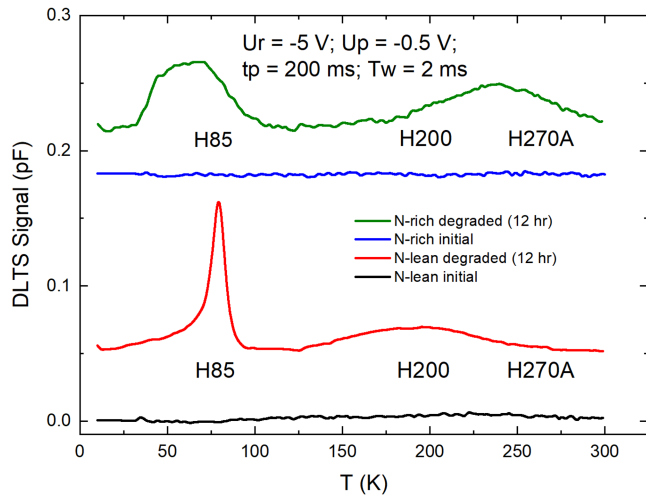| Traps	H85	H270A	H270B	H200
Activation Energy (eV)	0.10	0.43	-	0.46
Apparent capture cross section (cm^2)	1.87×10^{-20}	1.01×10^{-17}	-	7.41×10^{-18}
N-rich defect concentration (cm^{-3})	2.87×10^{14}	2.12×10^{13}	-	2.26×10^{13}
N-lean defect concentration (cm^{-3})	1.83×10^{14}	2.45×10^{13}	-	7.88×10^{12}
Defect concentration ratios (rich/lean)	1.57	0.87	-	2.87

H270B is below the DLTS detection limit.

Fig. 12. DLTS spectra of N-rich and N-lean in nonstabilized group at their initial and degraded states, respectively.

samples may suggest nitrogen does not play a role. However, the stabilization process effuses nitrogen from samples, essentially converting the N-rich sample into a N-lean sample. Thus, both results could be explained by nitrogen playing a role in defect formation.

H85 and H270A (seen in Tables IV and V) were detected in the degraded samples in stabilized and nonstabilized group using DLTS.

H85 traps are more concentrated at the surface and has a low activation energy (0.1 eV) with a small apparent capture cross section (7.85×10^{-19} cm^2). Therefore, H85 is unlikely to directly account for LeTID. On a side note, H85 could be related to the LeTID precursor, a metal–hydrogen complex, that has been suggested to be electrically active but not recombination active [10]. Indeed, H85 is metastable, its concentration is greater near the surface (see Fig. 10) and is present in higher concentrations in nongettered samples (see Tables IV and V).

It is important to note that the traps reported in this work are all majority carrier traps and have very small capture cross sections, making them likely weak recombination centers in p-type samples. Minority carrier trap detection methods are required to identify what could be the recombination active traps responsible for LeTID to then precisely quantify their impact on the lifetime. DLTS depth-profiles indicate that H270A and H270B are bulk defects. H270A is within the uncertainty range of the LeTID-related defect observed in [15]. H270B is not observed in the nonstabilized degraded samples, as shown in

the Appendix. The stabilized samples have faster regeneration rates in stabilized than nonstabilized samples [30]; thus, H270B is unlikely to be directly related to LeTID but could be linked to the regeneration reaction. On the other hand, trap H200 is only observed in the nonstabilized group and its defect density ratio of N-rich and N-lean (see Table V) closely correlates to that of the nitrogen content (see Table I) in the as-grown FZ wafers and is not present in stabilized and degraded samples, suggesting that H200 is a nitrogen-related trap. Furthermore, as H200 was only detected in the degraded nonstabilized samples after carrier injection, H200 could be a carrier injection-dependent trap, and to the best of our knowledge, H200 has not been reported before.

V. CONCLUSION

In this work, we study the effect of nitrogen on P- and B-doped FZ samples subjected to carrier injection at a temperature of 75°C under 1 kW/m^2 illumination, a treatment usually applied to test for LeTID. Our results show that the degradation only occurs in B-doped samples and that the extent of LeTID in N-rich FZ silicon is significantly higher than in N-lean FZ silicon (particularly in nonstabilized samples). We also show that a stabilization procedure (oxidation and diffusion) increases the speed of the LeTID cycle.

Using DLTS, we measure three traps in common in N-rich and N-lean degraded FZ silicon, respectively. The three traps with activation energies of $E_t + E_\infty = 0.1$ (H85), 0.43 (H270A), and 0.39 eV (H270B) are detected in N-rich degraded samples, and $E_t + E_\infty = 0.1$ (H85), 0.43 (H270A), and 0.46 eV (H200) are observed in N-lean degraded samples. Such traps are only detectable in the degraded samples and are undetectable before the LeTID formation process or after lifetime recovery from LeTID. Trap H270A at 0.43 eV is most likely to be LeTID-related. H270A is a bulk defect, only present in the degraded state of the samples and its energy level is in the range expected for LeTID. H270B is only observed in the stabilized samples after long LeTID cycles. Thus, H270B could be associated with lifetime regeneration of LeTID. H270B and H200 are carrier-enhanced traps that are newly reported and only present in the carrier-injected samples with and without the stabilization process, respectively.

APPENDIX

The DLTS scans of the N-rich and N-lean samples for the nonstabilized group at their initial and degraded states ($\sim$12 h during the LeTID formation process) is shown in Fig. 12. There

are many traps observed in both samples; however, we focus only on the traps that we found in both samples. These are H85, H200, and H270A, as tabulated in Table V. Note that the peak coupled with H85 observed in the N-rich nonstabilized sample from the scan is different from H50, the energy level extracted from Arrhenius plot shows that the activation energy of this level is $E_t + E_\infty = 0.01$ eV above the valence band. In addition, H200 is a new level found not present in the stabilized group but in both degraded N-rich and N-lean samples in the nonstabilized group. There is also trap H230 in the N-rich degraded sample that is responsible for the large peak at 230 K.

ACKNOWLEDGMENT

REFERENCES

[1] K. Ramspeck et al., "Light induced degradation of rear passivated MC-SI solar cells," in *Proc. 27th Eur. Photovolt. Sol. Energy Conf.*, 2012, pp. 861–865.
[2] F. Fertig et al., "Mass production of p-type cz silicon solar cells approaching average stable conversion efficiencies of 22-345," in *Proc. 7th Int. Conf. Silicon Photovolt.*, 2017, pp. 338–345.
[3] D. Chen et al., "Evidence of an identical firing-activated carrier-induced defect in monocrystalline and multicrystalline silicon," *Sol. Energy Mater. Sol. Cells*, vol. 172, pp. 293–300, 2017.
[4] D. Chen et al., "Hydrogen induced degradation: A possible mechanism for light- and elevated temperature- induced degradation in n-type silicon," *Sol. Energy Mater. Sol. Cells*, vol. 185, pp. 174–182, 2018.
[5] T. Niewelt et al., "Light-induced activation and deactivation of bulk defects in boron-doped float-zone silicon," *J. Appl. Phys.*, vol. 121, no. 18, 2017, Art. no. 185702.
[6] H. C. Sio et al., "Light and elevated temperature induced degradation in p-type and n-type cast-grown multicrystalline and mono-like silicon," *Sol. Energy Mater. Sol. Cells*, vol. 182, pp. 98–104, 2018.
[7] D. Chen et al., "Hydrogen-induced degradation: Explaining the mechanism behind light- and elevated temperature-induced degradation in n- and p-type silicon," *Sol. Energy Mater. Sol. Cells*, vol. 207, 2020, Art. no. 110353.
[8] M. A. Jensen et al., "Assessing the defect responsible for LeTID: Temperature- and injection-dependent lifetime spectroscopy," in *Proc. IEEE 44th Photovolt. Specialist Conf.*, 2017, pp. 3290–3294.
[9] D. Bredemeier, D. C. Walter, and J. Schmidt, "Lifetime degradation in multicrystalline silicon under illumination at elevated temperature: Indications for the involvement of hydrogen," in *Proc. AIP Conf.*, 2018, Art. no. 130001.
[10] J. Schmidt, D. Bredemeier, and D. C. Walter, "On the defect physics behind light and elevated temperature-induced degradation (LeTID) of multicrystalline silicon solar cells," *IEEE J. Photovolt.*, vol. 9, no. 6, pp. 1497–1503, Nov. 2019.
[11] C. Vargas et al., "Recombination parameters of lifetime-limiting carrier-induced defects in multicrystalline silicon for solar cells," *Appl. Phys. Lett.*, vol. 110, no. 9, 2017, Art. no. 092106.
[12] K. Nakayashiki et al., "Engineering solutions and root-cause analysis for light-induced degradation in *p*-type multicrystalline silicon PERC modules," *IEEE J. Photovolt.*, vol. 6, no. 4, pp. 860–868, Jul. 2016.
[13] A. E. Morishige et al., "Lifetime spectroscopy investigation of light-induced degradation in p-type multicrystalline silicon PERC," *IEEE J. Photovolt.*, vol. 6, no. 6, pp. 1466–1472, Nov. 2016.
[14] T. Mchedlidze and J. Weber, "Location and properties of carrier traps in Mc-Si solar cells subjected to degradation at elevated temperatures," *Physica Status Solidi (a)*, vol. 216, no. 17, 2019, Art. no. 1900142.
[15] S. Johnston et al., "Letid-affected cells from a utility-scale photovoltaic system characterized by deep level transient spectroscopy," in *Proc. IEEE 48th Photovolt. Specialists Conf.*, 2021, pp. 2276–2278.
[16] J. A. T. De Guzman et al., "Electronic properties and structure of boron-hydrogen complexes in crystalline silicon," *Sol. RRL*, vol. 6, no. 5, 2022, Art. no. 2100459.
[17] W. von Ammon, P. J. Dreier, W. Hensel, U. Lambert, and L. Köster, "Influence of oxygen and nitrogen on point defect aggregation in silicon single crystals," *Mater. Sci. Eng. B- Adv. Funct. Solid-state Mater.*, vol. 36, pp. 33–41, 1996.
[18] T. Abe and H. Takeno, "titleDynamic behavior of intrinsic point defects in FZ and CZ silicon crystals," *MRS Proc.*, vol. 262, pp. 3–13, 1992.
[19] C. R. Alpass, J. D. Murphy, R. J. Falster, and P. R. Wilshaw, "Nitrogen diffusion and interaction with dislocations in single-crystal silicon," *J. Appl. Phys.*, vol. 105, no. 1, 2009, Art. no. 013519.
[20] Y. Yatsurugi, N. Akiyama, Y. Endo, and T. Nozaki, "Concentration, solubility, and equilibrium distribution coefficient of nitrogen and oxygen in semiconductor silicon," *J. Electrochem. Soc.*, vol. 120, no. 7, 1973, Art. no. 975.
[21] K. Sumino, I. Yonenaga, M. Imai, and T. Abe, "Effects of nitrogen on dislocation behavior and mechanical strength in silicon crystals," *J. Appl. Phys.*, vol. 54, no. 9, pp. 5016–5020, 1983.
[22] K. Nauka, M. S. Goorsky, H. C. Gatos, and J. Lagowski, "Nitrogen-related deep electron traps in float zone silicon," *Appl. Phys. Lett.*, vol. 47, no. 12, pp. 1341–1343, 1985.
[23] Y. Tokumaru, H. Okushi, T. Masui, and T. Abe, "Deep levels associated with nitrogen in silicon," *Japanese J. Appl. Phys.*, vol. 21, no. 7A, pp. L443–L444, Jul. 1982.
[24] T. Abe, H. Harada, N. Ozawa, and K. Adomi, "Deep level generation-annihilation in nitrogen doped FZ crystals," *MRS Proc.*, vol. 59, pp. 537–544, 1985.
[25] K. Kakumoto and Y. Takano, "Deep level induced by diffused N2 and vacancy complex in SI," in *Proc. 2nd Int. Symp. Adv. Sci. Technol. Silicon Mater.*, 1996, p. 437.
[26] T. Niewelt et al., "Taking monocrystalline silicon to the ultimate lifetime limit," *Sol. Energy Mater. Sol. Cells*, vol. 185, pp. 252–259, 2018.
[27] Z. Hameiri et al., "Should the refractive index at 633 nm be used to characterize silicon nitride films?," in *Proc. IEEE 43rd Photovolt. Specialists Conf.*, 2016, pp. 2900–2904.
[28] R. A. Sinton et al., "A quasi-steady-state open-circuit voltage method for solar cell characterization," in *Proc. 16th Eur. Photovolt. Solar Energy Conf.*, 2000, pp. 1–4.
[29] S. Glunz, S. Rein, W. Warta, J. Knobloch, and W. Wettling, "Degradation of carrier lifetime in CZ silicon solar cells," *Sol. Energy Mater. Sol. Cells*, vol. 65, no. 1, pp. 219–229, 2001.
[30] D. Sperber, A. Heilemann, A. Herguth, and G. Hahn, "Temperature and light-induced changes in bulk and passivation quality of boron-doped float-zone silicon coated with sinx:H," *IEEE J. Photovolt.*, vol. 7, no. 2, pp. 463–470, Mar. 2017.
[31] D. Macdonald, L. J. Geerligs, and A. Azzizi, "Iron detection in crystalline silicon by carrier lifetime measurements for arbitrary injection and doping," *J. Appl. Phys.*, vol. 95, no. 3, pp. 1021–1028, 2004.
[32] C. Chan et al., "Modulation of carrier-induced defect kinetics in multicrystalline silicon PERC cells through dark annealing," vol. 1, no. 2, pp. 12–18, 2017.
[33] G. D. Watkins, "Intrinsic defects in silicon," *Mater. Sci. Semicond. Process.*, vol. 3, no. 4, pp. 227–235, 2000.
[34] W. Kwapil, T. Niewelt, and M. C. Schubert, "Kinetics of carrier-induced degradation at elevated temperature in multicrystalline silicon solar cells," in *Proc. 7th Int. Conf. Crystalline Silicon Photovolt., Sol. Energy Mat. Solar Cells*, 2017, pp. 80–84.
[35] W. von Ammon et al., "The impact of nitrogen on the defect aggregation in silicon," *J. Cryst. Growth*, vol. 226, no. 1, pp. 19–30, 2001.
[36] O. Engström and A. Alm, "Thermodynamical analysis of optimal recombination centers in thyristors," *Solid-State Electron.*, vol. 21, no. 11, pp. 1571–1576, 1978.
[37] J. Orton and P. Blood, *The Electrical Characterization of Semiconductors: Majority Carriers and Electron States*. London, U.K.: Academic Press, 1992.
[38] L. Dobaczewski, P. Kaczor, I. Hawkins, and A. Peaker, "Laplace transform deep-level transient spectroscopic studies of defects in semiconductors," *J. Appl. Phys.*, vol. 76, no. 1, pp. 194–198, 1994.
[39] D. Hiller et al., "Kinetics of bulk lifetime degradation in float-zone silicon: Fast activation and annihilation of grown-in defects and the role of hydrogen versus light," *Physica Status Solidi (a)*, vol. 217, no. 17, 2020, Art. no. 2000436.
[40] T. Itoh and T. Abe, "Diffusion coefficient of a pair of nitrogen atoms in float-zone silicon," *Appl. Phys. Lett.*, vol. 53, no. 1, pp. 39–41, 1988.
[41] R. Hull, *Properties of Crystalline Silicon*. London, U.K.: INSPEC, 1999.